AIChE

A CFD Study on the Effect of the Characteristic Dimension of Catalytic Wall Microreactors

G. Arzamendi, I. Uriz, A. Navajas, P. M. Diéguez, and L. M. Gandía
Departamento de Química Aplicada, Edificio de los Acebos, Universidad Pública de Navarra, Campus de Arrosadía s/n, E-31006 Pamplona, Spain

M. Montes
Grupo de Ingeniería Química, Departamento de Química Aplicada, Facultad de Ciencias Químicas de San Sebastián, UPV/EHU, Paseo Manuel de Lardizábal 3, 20018 San Sebastián, Spain

M. A. Centeno and J. A. Odriozola
Instituto de Ciencia de Materiales de Sevilla, Centro Mixto CSIC-Universidad de Sevilla, Avda. Américo Vespucio 49, 41092 Sevilla, Spain

DOI 10.1002/aic.12790
Published online October 21, 2011 in Wiley Online Library (wileyonlinelibrary.com).

A three-dimensional computational fluid dynamics study of the steam methane reforming (SMR) in microreactors is presented. Emphasis has been made on investigating the effects of the characteristic dimension (d: 0.35, 0.70, 1.40, and 2.80 mm) on the performance of two microreactor geometries: square microchannels and microslits. Results have shown that for both geometries the SMR conversion decreases markedly as d increases. Conversely, the microchannels provide a methane conversion slightly higher than that of the microslits. The different performance of the microreactors is only partially due to the different surface-to-volume ratio. Pronounced transverse temperature and concentration gradients develop as the characteristic dimension increases especially for microslits in the first half of the reactor. Therefore, external transport limitations can affect the performance of microreactors for SMR, although the characteristic dimensions are of the order of very few millimeters. © 2011 American Institute of Chemical Engineers *AIChE J,* 58: 2785–2797, 2012
Keywords: catalytic wall microreactor, computational fluid dynamics, methane steam reforming, microchannel reactor, microreactor

Introduction

Among the existing technologies for hydrogen production, namely, thermochemical (reforming, pyrolysis, and gasification of hydrocarbon fuels and coal), electrochemical (water electrolysis), and biological (anaerobic fermentation), the thermochemical route through the steam reforming of natural gas is the most economical and widely used accounting for about half the hydrogen produced globally.[1,2] Conversely, although hydrogen production for fuel cell applications is an emerging market, it is expected that the production needs increase largely in the future.[3] As a result, there is a great interest in the intensification of the steam methane reforming (SMR) to address some problems of the conventional process as efficiency, diffusional limitations, catalyst stability, and pollutant emissions.[4]

SMR in large centralized plants is a mature and well-optimized technology. Nevertheless, with a view to a future widespread implantation of hydrogen in the transportation sector, the challenges posed by the distribution of this fuel make reasonable to expect that during the transition to a hydrogen economy hydrogen would be produced locally, for example, at fuelling stations.[5] Distributed production of hydrogen will require the use of small-scale steam reformers that should be highly efficient, compact, durable, and easy to integrate with fuel cells; they should be characterized by very short startup times as well.[6] Miniaturization through the use of microreactors and multifunctional process equipment has the potential to be able to greatly contribute to this goal.[7] It is well-known that miniaturization leads to significant increases of transport rates.[8,9] This is particularly important in SMR because this reaction is usually heat transfer controlled, and it is also characterized by low effectiveness factors due to the interparticle temperature gradients established in the catalyst beds.[10] SMR is highly endothermic and is performed industrially in multiple packed-bed tubular reactors at temperatures above 900°C, so, a key issue is to achieve very high heat transfer rates.[3,11,12] There are several additional incentives for using microreaction technology in the SMR:[4,11–19] (1) it is possible to conduct the reaction at very short contact times, of the order of milliseconds, which favors reforming over the polymerization reactions leading to coke formation that are slower; (2) the hydrogen/syngas produced can be cooled quickly to prevent re-equilibration and carbon formation through the Boudouard reaction; (3) microreactors allow easy thermal integration through the

Correspondence concerning this article should be addressed to L. M. Gandía at lgandia@unavarra.es.

coupling of the endothermic SMR with the exothermic catalytic combustion of a fuel as natural gas, hydrogen, or mixtures thereof, thus, improving the thermal efficiency of the process and lowering the NO_x emissions; (4) miniaturization can open SMR up to new applications as onboard production of hydrogen or remote and offshore conversion of natural gas into synthetic liquid fuels through the gas-to-liquids process.

The steam methane reforming in microreactors has been investigated by several researchers. The Velocys® group[11,14] has developed technology for the SMR in compact microchannel reactors that achieves a very high degree of intensification of the heat transfer rate resulting in volumetric thermal fluxes above 65 W/cm^3 that clearly surpass the typical values (1 W/cm^3) of conventional reformers. This feature results in significant cost savings and the possibility of operating the microreformers at very short residence times. The improved heat and mass transfer rates achieved with a suitable design of the microchannel reactor make possible that the reaction enters the kinetic regime thus allowing to exploit in full the properties of very active SMR catalysts resulting in contact times below 1 ms instead of 1 s, which is a typical value in conventional reformers.[15] Stefanidis and Vlachos[19] stated that heat transfer enhancement is insufficient for SMR intensification, being also necessary "catalyst-intensification." Seris et al.[16] built and operated a plant at pilot scale based on plate modules containing microchannels capable of producing 5 Nm^3/h of hydrogen from the steam reforming of desulfurized natural gas. Ryi et al.[20] designed and manufactured a microreformer based on plates with microchannels that produced sufficient hydrogen from the SMR reaction as to feed a 26-W polymer electrolyte membrane fuel cell. Cao et al.[21] developed a methane steam microreformer based on FeCrAlY felts containing a Rh catalyst capable of operating at space velocities as high as 3,600,000 h^{-1}.

As concerns the modeling and simulation of the thermal coupling of the SMR and methane combustion reactions in compact systems, the first mathematical models focused on the counter-current arrangement. These models were one-dimensional (1-D) and relatively oversimplified due to the mathematical difficulties introduced by the excessive maximum temperatures that appear in the middle of the reactor and their effect on the highly nonlinear reaction rate expressions. These studies showed that it is necessary to establish an optimal overlapping of the reaction zones for controlling the reaction temperature.[22] Most of the subsequent models considered the cocurrent arrangement. Zanfir and Gavriilidis[23] developed a 2-D model of a catalytic plate reactor, in which the SMR and methane catalytic combustion take place in alternate channels for cocurrent flow arrangement. It was shown that the short distances between the heat sources and sinks prevailing in microreactors result in very low transverse temperature gradients across the walls and gas phase. These authors reported that the reduction of the transport limitations had an overall effect of reducing the reactor volume and catalyst weight by two orders of magnitude compared to conventional steam methane reformers. Two-dimensional models of microreactors consisting of parallel catalytic plates coupling the SMR and the catalytic combustion of a gaseous fuel in cocurrent flow configuration have been developed also by Stefanidis and Vlachos[17–19] to investigate the effects on the microreformer performance of the characteristic length scale, contact time, wall material, fuel, and reforming catalyst. Finally, 3-D models and computational fluid dynamics (CFD) simulations have been performed by Vaccaro et al.[24,25] and Mettler et al.[12,26] to study the issue of external heat losses and their influence on the stability and scale-out of microreactors coupling the SMR and methane combustion reactions.

In a previous paper,[27] we reported on a 3-D CFD study of the SMR in a microchannel reactor coupled with the catalytic combustion of methane in air. The effects on the microreactor performance of the SMR and combustion reactions space velocities, load of the reforming catalyst, steam-to-carbon ratio, and flow arrangement (cocurrent and cross-flow) were discussed in detail. In this work, a new CFD simulation study on this system is presented with the aim of investigating the influence of the characteristic dimension on the performance of two geometries with very different aspect ratios: square microchannels and microslits that can be considered also as plate microreactors.

CFD Model and Simulation Conditions

Three-dimensional CFD simulations were performed using ANSYS® CFX software on a Dell Precision PWS690 workstation running MS Windows XP® × 64 with an available random-access memory (RAM) of 16.0 GB. In the previous works, the models developed with this software tool have provided reliable results for a variety of reacting systems in microreactors: methane,[27] methanol,[28] and ethanol[29] steam reforming, heat transfer in the low-temperature Fischer–Tropsch synthesis,[30] and more recently, preferential oxidation (PROX) of CO.[31,32]

Two physical models have been included in this study. The first model consisted of a steel block with four square parallel microchannels of 20 mm of length and 0.35, 0.70, 1.4, and 2.8 mm of side (d). It is considered that the SMR reaction takes place in two of the channels and the combustion of methane in the other two. The second was a model for a geometry consisting of a steel block with two parallel microslits, one for each reaction, of 20 mm of length. In this case, heights (d) of 0.35, 0.70, 1.4, and 2.8 mm have been considered. As concerns the microslits width, it is necessary to establish some reference to be able to perform comparisons due to the very different aspect ratios of both microchannels and microslits. In this regard, the width was adjusted for each value of d to obtain a total internal wall surface area of 560 mm^2, that is, equivalent to the wall surface area of 10 square microchannels of 0.7 mm of side, a pattern that is being used by our group to fabricate microreactors for several applications.[32–34] The geometries of the microslits are shown in Figure 1 and their dimensions are compiled in Table 1, where the aspect ratio (α, depth/width) is also included. As a consequence of the reference adopted, the sum of the depth and width of the microslits is constant and equal to 14 mm; therefore, their width decreases slightly as the characteristic dimension increases. Conversely, the hydraulic diameter of the microslits is within the 0.68–4.48 mm range, that is, slightly lower than the double of d.

As concerns the CFD model, ANSYS® CFX software is based on the finite volume method and uses a fully implicit coupled solver. The governing equations and main features of the model developed are summarized in Table 2. Governing equations included the transport equations for total mass, momentum, thermal energy and species, and the ideal gas

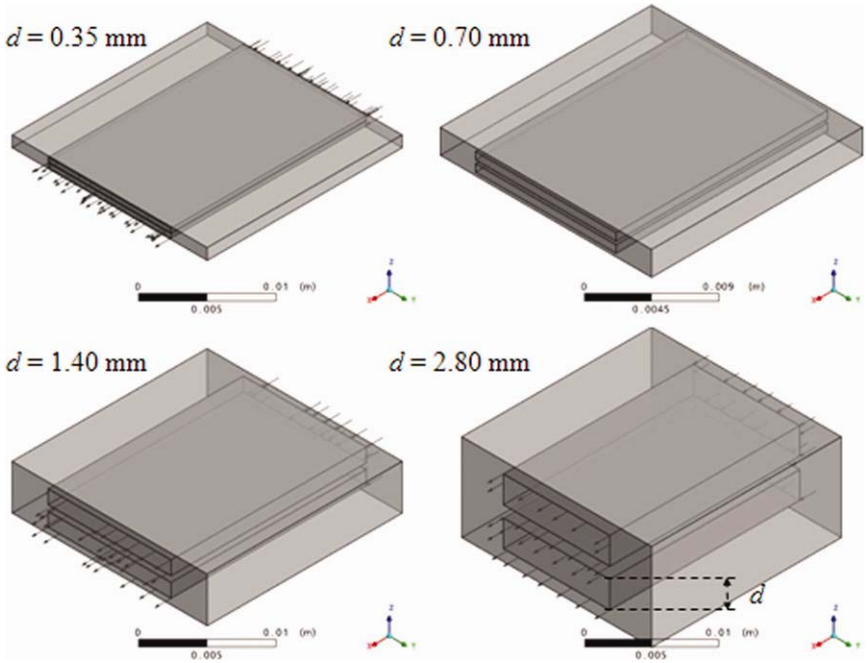

Figure 1. Geometries showing the solid and fluidic domains of the parallel microslits considered in this study.

[Color figure can be viewed in the online issue, which is available at wileyonlinelibrary.com.]

equation of state. Spatial discretization was performed according to the first-order upwind differencing scheme (UDS), which is unconditionally stable and accurate.[35] Criteria of convergence were based on the residuals defined as the normalized root mean square (RMS) of the difference between the latest solution and the running arithmetic average of the variables. Maximum RMS residuals were set at 10^{-5}. Because of the very fast kinetics of the methane combustion at the prevailing reaction temperatures, it has been necessary to adopt a conservative approach to achieve numerical stability and convergence. In this regard, timescale (under-relaxation) factors of 0.01 were applied to the internally calculated auto timescales for the thermal energy and species equations. Under these conditions and with the grids adopted in this work, the imbalance level of the conservation equations after convergence was typically below 1%.

In view of the characteristics of the geometrical models, structured meshes were created in the fluidic domains with ANSYS® Mechanical APDL software. This code is capable of creating 3-D structured mesh consisting of hexahedral cells. To this end, 2-D meshes were constructed first, and then, they were extruded along the appropriate axis. In this way, the whole computational domain is as orthogonal as possible to reduce the truncation errors and computation time. Regular meshes are very convenient, when using first-order UDS for discretization to minimize numerical errors due to the tendency of this scheme to numerical diffusion.[35] Stretched grids were developed with a larger number of elements near the walls, where the most pronounced changes of the transport properties can be expected. Mesh independence tests have been performed to ensure that the solutions do not vary with the number of computational elements. We concluded that about 100,000–150,000 volume elements provided mesh-independent solutions. The meshes finally developed for the blocks of microchannels and microslits with characteristic dimension $d = 0.70$ are shown in Figures 2A (95,040 elements) and B (150,720 elements), respectively. As for the boundary conditions, to establish flow direction, the entrances to the microchannels and microslits were considered as inlets with uniform properties (velocity, temperature, pressure, and composition), whereas the exits were set as constant pressure (1 atm) outlets. The external walls of the microreactor block were considered adiabatic and the internal walls of the microchannels and microslits, where the catalyst is placed, as nonslip sources of products and sinks of reactants to model the heterogeneously catalyzed reactions. It has been assumed that thin and homogeneous layers of typical Ni (2 mg/cm^2) and Pd/Al_2O_3 (1 mg/cm^2) catalysts were deposited onto the walls of the SMR and methane combustion ducts, respectively. These loadings per unit surface area have been maintained constant for both geometries, and the several characteristic dimensions. As concerns the kinetics, rate expressions were taken from the literature for the SMR,[36] water–gas shift (WGS),[37] and methane

Table 1. Dimensions of the Microslits*

Height (mm)	Width (mm)	Hydraulic Diameter (mm)	Surface-to-Volume Ratio (mm^{-1})	Aspect Ratio (α, depth/width)
0.35	13.65	0.68	5.86	0.03
0.70	13.30	1.33	3.01	0.05
1.40	12.60	2.52	1.59	0.11
2.80	11.20	4.48	0.89	0.25

*The microslits length and total wall surface area were kept constant at 20 mm and 560 mm^2, respectively.

Table 2. CFD Model Features

Description	Equation/Setting/Value
Steady state governing equations	
Continuity equation	$\nabla\cdot(\rho\cdot\boldsymbol{u})=0$
Momentum conservation	$\nabla\cdot(\rho\cdot\boldsymbol{u}\otimes\boldsymbol{u})=-\nabla p+\nabla\cdot\tau$ $\tau=\mu\left(\nabla\boldsymbol{u}+(\nabla\boldsymbol{u})^T-\frac{2}{3}\delta\nabla\cdot\boldsymbol{u}\right)$
Thermal energy	$\nabla\cdot(\rho\cdot\boldsymbol{u}\cdot h)=\nabla\cdot(\lambda\cdot\nabla T)+\tau\colon\nabla\boldsymbol{u}+S_{\mathrm{E}}$ $h=\sum_{i}^{N_s}Y_{\mathrm{i}}\cdot h_{\mathrm{i}}$ $h_{\mathrm{i}}=h_{\mathrm{i},T_{\mathrm{ref}}}+\int_{T_{\mathrm{ref}}}^{T}c_{\mathrm{p,i}}dT$ $S_{\mathrm{E}}=\sum_{j=1}^{N_r}(-\Delta H_{\mathrm{R}})_j\cdot R_j$
Species mass balance	$\nabla\cdot(\rho\cdot\boldsymbol{u}\cdot Y_{\mathrm{i}})=\nabla\cdot(\rho\cdot D_{\mathrm{i,mix}}\cdot\nabla Y_{\mathrm{i}})+S_{\mathrm{i}}$ $S_{\mathrm{i}}=\sum_{j=1}^{N_r}\upsilon_{\mathrm{ij}}\cdot R_{\mathrm{j}}$
Ideal gas equation of state	$\rho=\frac{p\cdot M}{R\cdot T}$
Steam methane reforming (SMR)[36]	$R_{\mathrm{SMR}}=\frac{3.06\times10^5\cdot\exp(-15600/T)}{1+0.5\cdot P_{\mathrm{H_2O}}/P_{\mathrm{H_2}}+20\cdot P_{\mathrm{CO}}}\cdot P_{\mathrm{CH_4}}$
Methane combustion (MC)[38]	$R_{\mathrm{MC}}=2.84\times10^8\cdot\exp(-131000/T)\cdot y_{\mathrm{CH4}}^{0.72}$
Meshing	
Mesh type	Structured (fluidic domains)
Number of finite-volume cells	$\approx$ 100,000–150,000
Boundary conditions	
Entrance	Uniform velocity, temperature and pressure inlet
Exit	Constant pressure (1 atm) outlet
Inner walls	Nonslip, sources and sinks of species
External walls	Adiabatic
Solver	
Discretization scheme	First-order upwind
Timescale	1% of the auto timescale for the energy and species
Convergence criteria	RMS residuals $<10^{-5}$

combustion[38] reactions. These expressions are source terms in the species transport equation of the CFD model as indicated in Table 2. Homogeneous reactions were neglected for the steam reforming process, whereas some simulations revealed that the homogeneous combustion of methane is not significant under the conditions prevailing in this work.[27]

Simulations were performed at steady state and considering parallel cocurrent flow arrangement. The steam-to-carbon (S/C) molar ratio of the SMR feed was set at 2, that is, twice the stoichiometric value to simulate conditions that prevent coke formation on the catalyst surface. The inlet temperatures of the reforming and combustion gas feed streams were established at 600°C, which is a typical SMR inlet temperature.[39] For the fuel, the composition was set at 2 wt % methane in air to obtain a mixture with a methane content sufficiently below the lower flammability level. The ratio between the mass flow rates of the fuel and steam reforming streams was maintained throughout this study at 5.06, which ensures the achievement of high SMR conversions in a wide range of operating conditions.

Results and Discussion

Effect of the characteristic dimension, geometry, and space velocity

The mean methane steam reforming conversion at the microreactor outlet as a function of the SMR gas hourly space velocity (GHSV) and the characteristic dimension of the microchannels and microslits are shown in Figures 3A and B, respectively. GHSV has been defined as the volumetric feed flow rate referred to standard pressure and temperature divided by the microchannels or microslits volume. As expected, the SMR conversion decreases with the space velocity. Also, it can be seen that for both geometries, the reforming conversion decreases markedly as the characteristic dimension increases within the 0.35–2.80 mm range. At a space velocity of, for example, 20,000 h^{-1}, the mean methane conversion achieved by the microchannels decreases from 95.3 to 90.9 and 85.2% as the characteristic dimension increases from 0.35 to 0.70 and 1.40 mm, respectively. At the same GHSV of 20,000 h^{-1}, the methane conversion decreases in the case of the microslits from 90.5 to 84.9%, when d increases from 0.35 to 0.70 mm. Therefore, the microchannels provide a methane conversion significantly higher than that of the microslits at a given GHSV. The differences between the performances of these geometries increase with the space velocity. As a result, only the microchannels allow obtaining significantly high methane conversions at very high GHSVs. For example, the microchannel

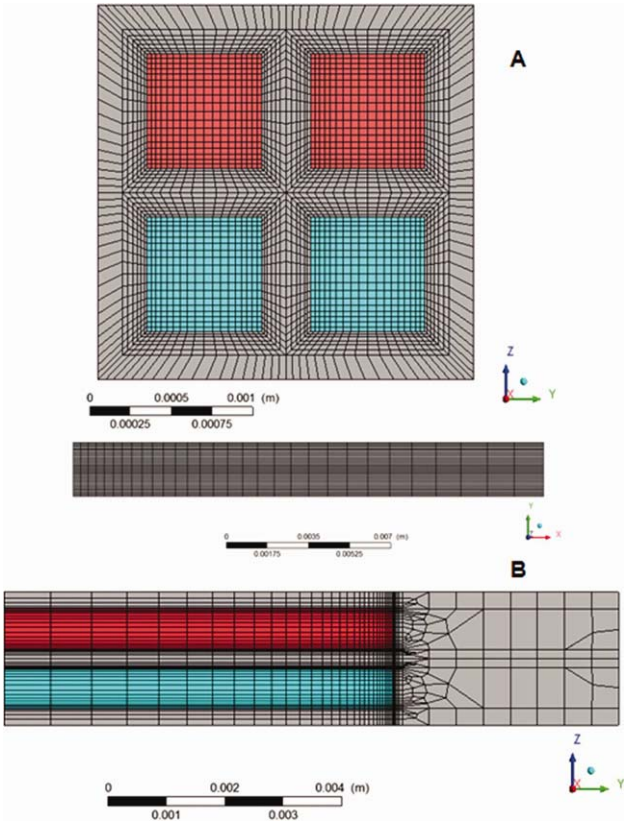

Figure 2. Meshes developed for the microchannel (A) and microslit (B) reactors with characteristic dimension of 0.7 mm.

Colored regions correspond to the fluidic domains. [Color figure can be viewed in the online issue, which is available at wileyonlinelibrary.com.]

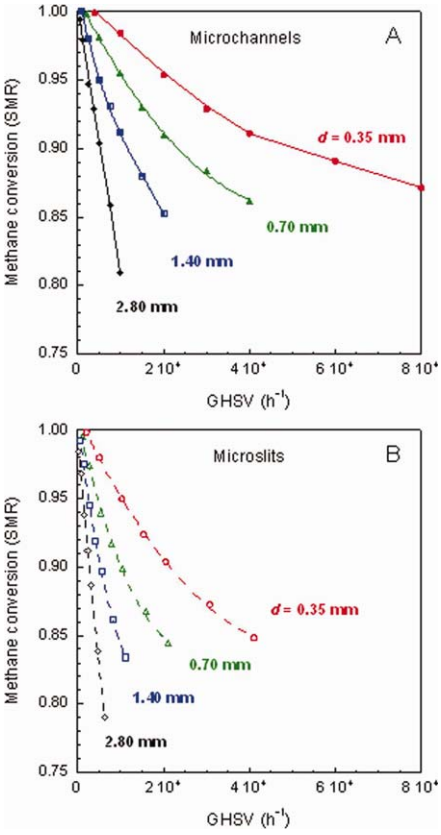

Figure 3. Effect of the reforming GHSV and characteristic dimension (*d*) on the mean methane steam reforming conversion at the outlet of the microchannels (A) and microslits (B).

[Color figure can be viewed in the online issue, which is available at wileyonlinelibrary.com.]

with the smallest *d* provides a methane conversion of 87% at a SMR space velocity as high as 80,000 h^{-1} (Figure 3A). In the case of the smallest microslit, the methane steam reforming conversion of 88% can be achieved at the much lower GHSV of 30,000 h^{-1} (Figure 3B) thus resulting that the throughput provided by the microchannel is 2.7 times higher than that of the microslit. When similar calculations are made for a SMR conversion of 88% and other characteristic dimensions it results that the throughputs achievable with the microchannels are 2.4, 2.2, and 1.8 times higher than that of the microslits as the characteristic dimension increases from 0.70 to 1.40 and 2.80 mm, respectively. These results also evidence that the differences between the performances of both geometries are less marked as their characteristic dimensions increase.

The evolution of the mean outlet reforming and methane combustion temperatures as a function of the reforming GHSV and the characteristic dimension of the microchannels and microslits are depicted in Figures 4A and B, respectively. The outlet temperatures are approximately between 850 and 950°C, which are typical SMR temperatures. Also, it can be seen that the evolution of the outlet reforming temperature is opposite to that of the SMR conversion. Indeed, the temperature increases as both the space velocity and the characteristic dimension increase. To understand this behavior, it has to be taken into account that the ratio between the mass flow rates of the fuel and the reforming streams and the inlet temperature (600°C) were maintained constant in all the simulations performed. Moreover, the conversion of the methane combustion reaction at the microreactors outlet was 100% in all cases except for the biggest microchannel at GHSV of 10,000 h^{-1} (96%) and the biggest microslit at GHSVs of 4686 h^{-1} (99%) and 6249 h^{-1} (97%). Nevertheless, even in these cases the methane combustion conversions were very high. Therefore, it can be considered that the heat available per mol of methane fed to the microreactor was the same in all cases. As evidenced in Figure 5A, the outlet reforming temperature increases as the SMR conversion decreases because less heat is consumed by the reforming reaction turning out that more energy is available as sensible heat. It can be seen also in Figure 5A that for a given SMR conversion the outlet temperature is very similar regardless of the characteristic dimension and geometry (microchannels or microslits). This is an expected result for an adiabatic reactor provided that methane combustion is complete, that is, that the heat available per mol of methane fed was the same in all cases. As a matter of fact, only the cases for which methane combustion was incomplete (marked by arrows in Figure 5A) deviate from the trend giving rise to lower exit temperatures. Apart from these cases, the small temperature differences are mainly attributed to numerical errors.

The mean outlet temperatures of the methane combustion reaction (indicated by + symbols in Figures 4A and B) were

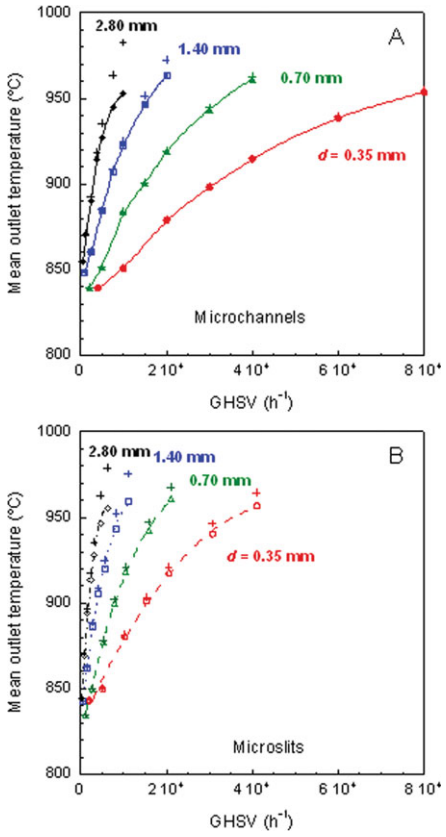

Figure 4. Evolution of the mean SMR and methane combustion (+ symbols) temperatures as a function of the reforming GHSV and characteristic dimension at the outlet of the microchannels (A) and microslits (B).

[Color figure can be viewed in the online issue, which is available at wileyonlinelibrary.com.]

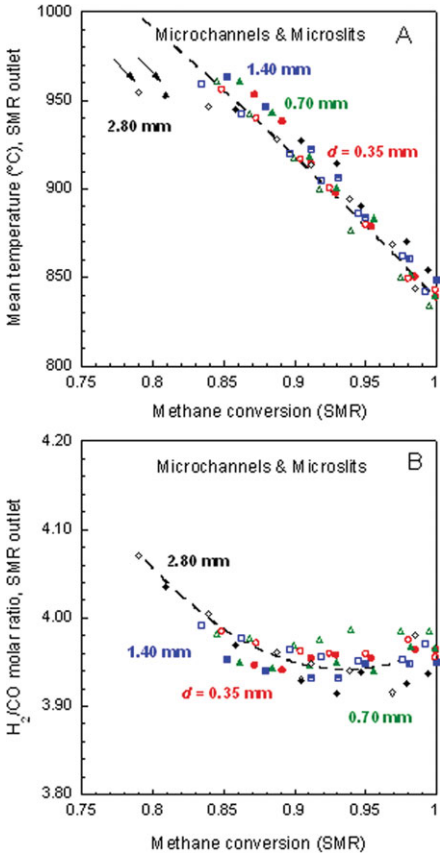

Figure 5. Evolution of the mean SMR temperature (A) and H_2/CO molar ratio (B) as a function of the mean methane steam reforming conversion and characteristic dimension at the outlet of the microchannels (closed symbols) and microslits (open symbols). Arrows indicate cases of incomplete methane combustion.

[Color figure can be viewed in the online issue, which is available at wileyonlinelibrary.com.]

always higher than that of the SMR. The differences between these temperatures were low but increased with the space velocity and the characteristic dimension. In the case of the microchannels, the maximum difference varied between only 1°C for $d = 0.35$ mm and 31°C for the biggest microchannel, whereas for the microslits it varied between 7°C when $d = 0.35$ mm and 24°C if $d = 2.80$ mm.

The selectivity to hydrogen has been evaluated through the mean H_2/CO molar ratio at the microreactors outlet that is shown as a function of the SMR methane conversion and the characteristic dimension of the microchannels and microslits in Figure 5B. The stoichiometric value of the molar H_2/CO ratio for the SMR reaction is 3. Ratios above this value are due to the contribution of the WGS reaction. As can be seen in Figure 5B, the H_2/CO ratios in this study are between 3.9 and 4, which are typical values for the SMR when using feed streams with S/C ratios of 2.[27] The H_2/CO ratio goes through a smooth minimum as the methane conversion increases. This behavior can be understood as the result of the opposite effects of the methane conversion and the temperature on the WGS reaction. Indeed, at relatively low methane conversions the H_2/CO is high. This can be attributed to the lower consumption of water at low methane conversions, and then, to the higher concentration of this reactant that favors the WGS. Consequently, as the SMR conversion increases both the excess of water and the H_2/CO ratio decreases. However, the WGS is an exothermic reversible reaction, whose equilibrium conversion is favored by relatively low temperatures. As discussed previously, the temperature decreases with the SMR conversion due to the higher consumption of the combustion heat by the endothermic reforming reaction. This fact could explain the small increase of the H_2/CO ratio taking place at very high SMR conversions.

Taking into account that the catalyst is deposited on the inner walls, it is possible that the different behavior may lie in the significantly different surface-to-volume ratio of the several microreactors. This was the case when studying by CFD simulations, the steam reforming of methanol in square channels with 0.35–1.40 mm of side as reported in a previous paper.[28] The surface-to-volume ratio of the square microchannels increases from 1.4 mm^{-1} for $d = 2.80$ mm to 11.4 mm^{-1} for $d = 0.35$ mm. As concerns the microslits, it can be seen in Table 1 that the surface-to-volume ratio increases from 0.89 mm^{-1} for $d = 2.80$ mm to 5.86 mm^{-1} for $d = 0.35$ mm. Therefore, for a given characteristic dimension the surface-to-volume ratio of the microchannels is higher than that of microslits, especially, when d is very low, which could explain the better performance exhibited by the microchannels compared to the microslits. Taking into consideration the different surface-to-volume ratio, the results have been compared on the basis of the weight hourly space velocity (WHSV), as shown in Figure 6. This variable has been calculated as the total mass flow rate of the feed stream divided by the catalyst weight, which is given by the product of the inner walls surface area and the catalyst loading referred to the unit surface area. As a result, for a given WHSV, the space time is constant if the catalyst loading and feed stream composition are also constant, irrespective of the characteristic dimension and channel geometry. When compared with the results in Figures 3A and B, Figure 6 shows that the differences are greatly reduced, especially at low space velocities. Nevertheless, still it is possible to observe that the methane conversion increases as the characteristic dimension decreases and that the

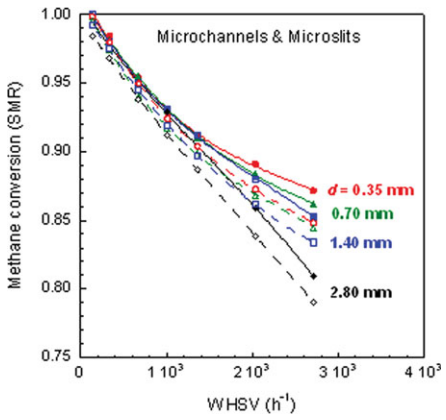

Figure 6. Effect of the reforming WHSV and the characteristic dimension on the mean methane steam reforming conversion at the microchannels (solid lines) and microslits outlet (dotted lines).

[Color figure can be viewed in the online issue, which is available at wileyonlinelibrary.com.]

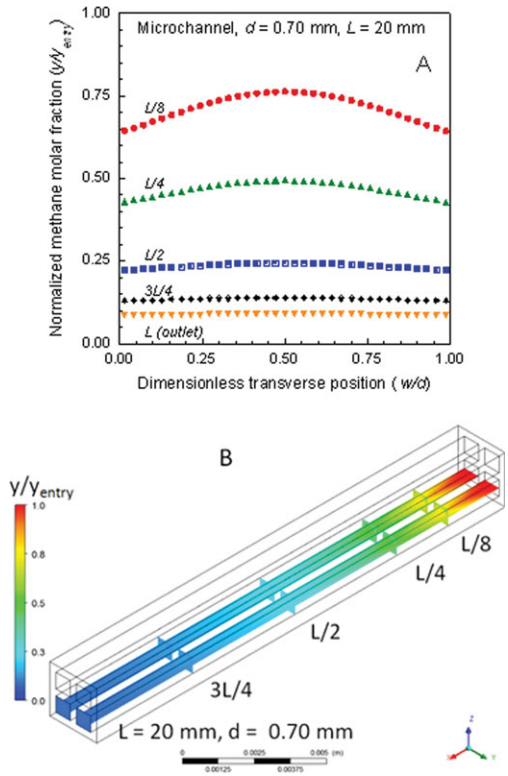

Figure 7. Normalized methane molar fraction in the reforming ducts of the microchannels with d = 0.70 mm at GHSV of 40,000 h^{-1} (WHSV = 2708 h^{-1}) and the indicated positions along the microchannel length: profiles along the dimensionless transverse position (A) and colored contours (B).

[Color figure can be viewed in the online issue, which is available at wileyonlinelibrary.com.]

microchannels allow obtaining higher methane conversions than the microslits. For example, at WHSV of 2711 h^{-1}, the mean SMR conversion at the microchannels outlet is about 87.1% when d is 0.35 but decreases to 86, 85.1, and 80.9% when the characteristic dimension increases up to 0.70, 1.40, and 2.80 mm. At this WHSV, the smallest microslit achieves a methane conversion of 84.8% that further decreases to 78.9% as d increases up to 2.80 mm. These results suggest that factors as, for example, the effect of possible transport limitations might have some influence on the microreactors performance as discussed in the next sections.

Influence of transport limitations. Microchannels

In this work, internal diffusion effects in the catalyst layers have been neglected due to the small thickness of the layers which, on the basis of the loadings of the SMR and methane combustion catalysts, are estimated to be about 20 and 10 μm, respectively.[29] The same assumption was made by Kölbl et al.,[40] for a 20-μm thick layer of a Pd–Zn/ZnO catalyst in a study on the examination of external mass transport in a microchannel reactor for the steam reforming of methanol. In the review by Walter et al.,[41] on mass transfer limitations in microchannel reactors, a study is reported in which internal mass transfer limitations were experimentally excluded for catalysts layers with thicknesses between 5 and 20 μm during the steam reforming of methanol. Evidently, the risk of transport limitations is much higher during the steam reforming of methane due to the very high operating temperatures that lead to fast chemical kinetics. As a matter of fact, Zanfir and Gavriilidis[23] have calculated effectiveness factors between 0.25 and 0.6 for the SMR reaction in a catalytic plate reactor containing a catalyst layer 20-μm thick. Being aware that internal transport effects might play a role under the conditions considered in this study we think that the assumption made does not affect significantly the conclusions drawn about the influence of the characteristic dimension which is the aim of this work.

To check if external (interphase) transport limitations are playing a role in the microreactors performance the possible presence of profiles of methane concentration in the gas phase has been first examined. To this end, the molar fraction of methane has been normalized with respect to its value at the microreactor entry. The evolution of the normalized methane molar fraction in a central plane along the width of the microchannel with d = 0.70 mm for a GHSV of 40,000 h^{-1} is represented in Figures 7A and B at the following positions (x) along the channel length: L/8, L/4, L/2, 3·L/4 and L, being L the total channel length (20 mm). The transverse position is expressed in dimensionless form referred to the total channel width (Figure 7A) that coincides with the characteristic dimension (d). In Figure 7B, the results are given in the form of colored contours. Obviously

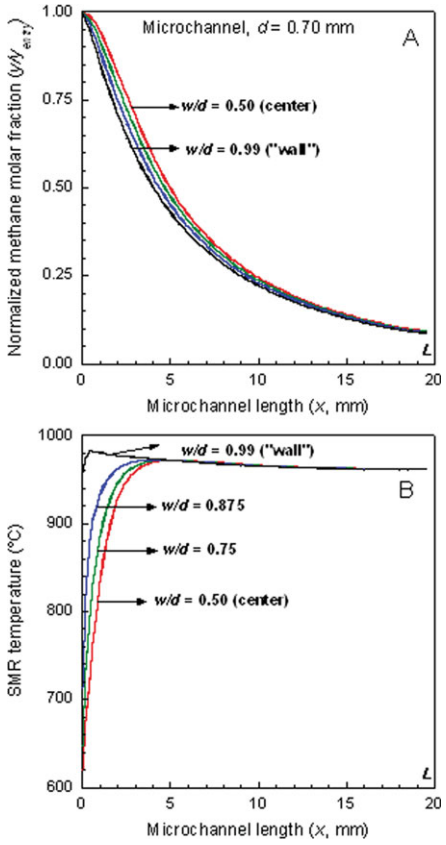

Figure 8. Evolution of the normalized methane molar fraction (A) and SMR temperature (B) along the microchannel length (d = 0.70 mm) at the dimensionless transverse positions indicated (GHSV = 40,000 h^{-1}, WHSV = 2708 h^{-1}).

[Color figure can be viewed in the online issue, which is available at wileyonlinelibrary.com.]

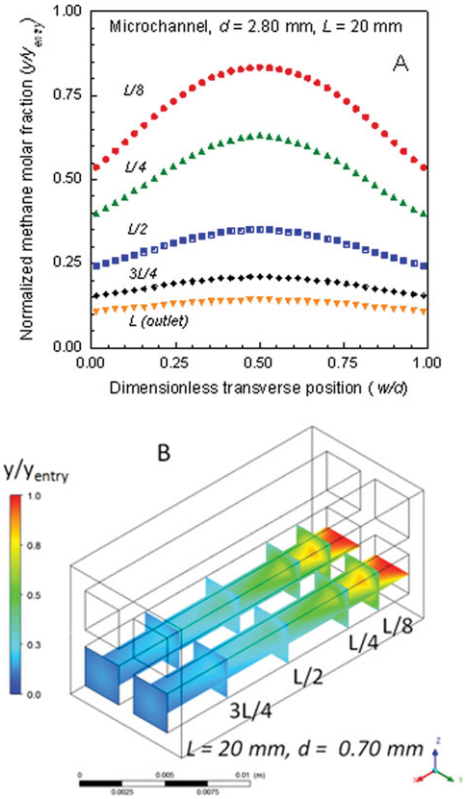

Figure 9. Normalized methane molar fraction in the reforming ducts of the microchannels with d = 2.80 mm at GHSV of 10,000 h^{-1} (WHSV = 2708 h^{-1}) and the indicated positions along the microchannel length: profiles along the dimensionless transverse position (A) and colored contours (B).

[Color figure can be viewed in the online issue, which is available at wileyonlinelibrary.com.]

the normalized methane concentration decreases with the SMR methane conversion so it also decreases along the microchannel. As can be seen, near the channel entry ($x = L/8$) there are smooth methane concentration profiles that practically disappear from half channel length. Methane is consumed at the channels walls where the catalyst is located; therefore, the profiles show a maximum at the center of the channel. These results are shown in a different way in Figure 8A where the evolution of the normalized methane molar fraction along the channel length at fixed values of the dimensionless transverse positions (w/d = 0.50, 0.75, 0.875, and 0.99) is depicted; $w/d = 0.50$ corresponds to the channel center, and $w/d = 0.99$ is a point very close to the channel wall. It can be seen that the curves do not overlap until approximately half channel length meaning that transverse concentration profiles exist near the entry although in this case they are not very marked. In Figure 8B, the evolution of the SMR temperature is shown. It can be seen that transverse temperature profiles are negligible from about a quarter of the channel length; moreover, from that point the temperature hardly changes so the reforming reaction is taking place almost isothermally. In contrast, very important differences of temperature develop near the channel entry. The temperature is very high close to the channel wall due to the proximity of the methane combustion channels whereas it is lower at the channel center although it increases quickly. Figures 9 and 10 show the results for a channel of d = 2.80 mm at GHSV = 10,000 h^{-1}. The most noticeable feature is the intense transverse concentration profiles that are established, especially along the first half of the channel length. These profiles are still appreciable even at the channel outlet as shown in Figure 10A where it can be seen that the curves do not overlap practically at any point along the channel length. As evidenced in Figure 10B transverse temperature profiles are also very marked and are maintained along the three quarters of the channel length. From these results, it is reasonable to attribute the worsening of the microchannels performance with the increase of the characteristic dimension to the heat and especially mass transport limitations prevailing in the biggest channels, particularly for the characteristic dimensions of 1.40 and 2.80 mm.

Zanfir and Gavriilidis[23] also found noticeable temperature and methane mass fraction transverse gradients in a numerical study based on a 2-D model of the SMR reaction coupled with the combustion of methane in a catalytic plate reactor. These authors considered characteristic dimensions (channel heights) between 1 and 4 mm. The smaller channel heights resulted in more efficient heat and mass transfer rates and less pronounced temperature and mass fraction gradients. The effects of the transport limitations were discussed in terms of the mass Fourier number (Fo), which is a

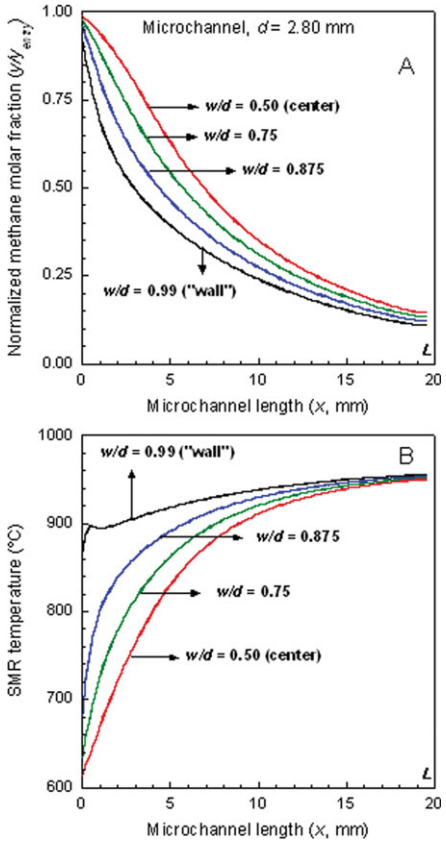

Figure 10. Evolution of the normalized methane molar fraction (A) and SMR temperature (B) along the microchannel length (d = 2.80 mm) at the dimensionless transverse positions indicated (GHSV = 10,000 h^{-1}, WHSV = 2708 h^{-1}).

[Color figure can be viewed in the online issue, which is available at wileyonlinelibrary.com.]

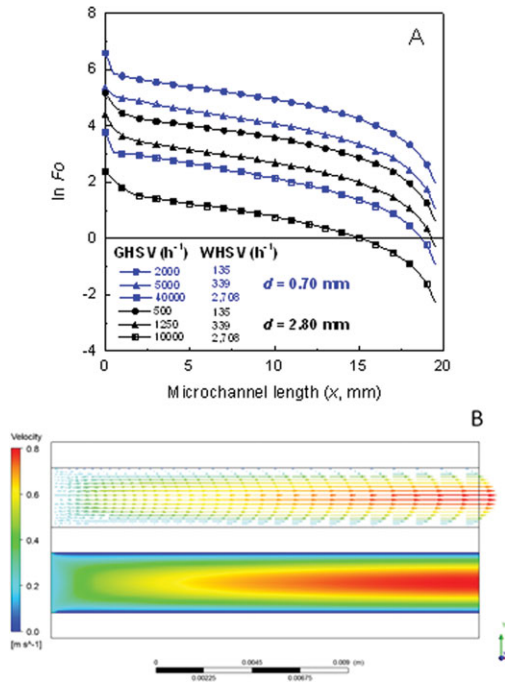

Figure 11. (A) Logarithm of the mass Fourier (*Fo*) number along the length of the SMR microchannels with *d* = 0.70 mm (blue symbols) and *d* = 2.80 mm (black symbols) at the GHSV and WHSV values indicated; (B) velocity profiles in a central plane of the microchannel with *d* = 2.80 mm at GHSV of 10,000 h^{-1} (WHSV = 2708 h^{-1}, *Re* = 17).

[Color figure can be viewed in the online issue, which is available at wileyonlinelibrary.com.]

function of the axial position (x) and can be used to evaluate, if the methane molecules have enough time to reach the catalytic wall from the channel center before they exit the reactor[23]

$$Fo = \frac{L - x}{u_x} \cdot \frac{D_{CH_4}(x)}{(d/2)^2} \tag{1}$$

where L is the channel or plate length (20 mm), u_x is the axial gas velocity, and D_{CH_4} (x) is the molecular diffusion coefficient of methane at the axial position considered. Fourier numbers above 1 (ln $Fo > 0$) indicate that the reactant molecules have enough time to reach the wall before exiting the microreactor. Fo numbers have been calculated for the SMR according to the above equation and the values of the logarithm of Fo along the length of the microchannels with characteristic dimension of 0.70 and 2.80 mm at several space velocities is shown in Figure 11A. Obviously, the Fo number decreases along the channel and, for a given size, it decreases as the GHSV increases. It can be seen, however, that the Fo numbers are significantly higher for the microchannel with d = 0.70 mm meaning that for that characteristic dimension the external mass transport limitations are of minor importance. Fo numbers lower than 1 (ln $Fo < 0$) have been obtained for the largest microchannel (d = 2.80 mm) at the space velocities of 10,000 and 1250 h^{-1}. In the first case, this happens from an axial position of 15.1 mm and in the second one from 19.2 mm. Therefore, the methane molecules in the center of this channel do not have enough time to reach the catalyst surface only after reaching three quarters of the channel length. For the microchannel with d = 0.70 mm, Fo number is lower than 1 at the very high GHSV of 40,000 h^{-1} and very near the channel exit (x = 18.7 mm).

Renken and Kiwi-Minsker[9] have extensively reviewed the several aspects of the microstructured catalytic reactors. As concerns the catalytic wall reactors, in addition to the internal and external transport limitation issues, these authors also emphasize the relevance of the flow pattern. Indeed, at the laminar regime usually prevailing in microreactors the radial diffusion favors mixing, whereas diffusion in the axial direction enhances the spread of the parabolic velocity profile affecting the residence time distribution and the microreactor performance. Axial dispersion is characterized by the Bodenstein number (Bo) that for microchannels can be estimated as follows[9]

$$Bo = 200 \cdot \tau \cdot \frac{D_{CH_4}}{d_h^2} \tag{2}$$

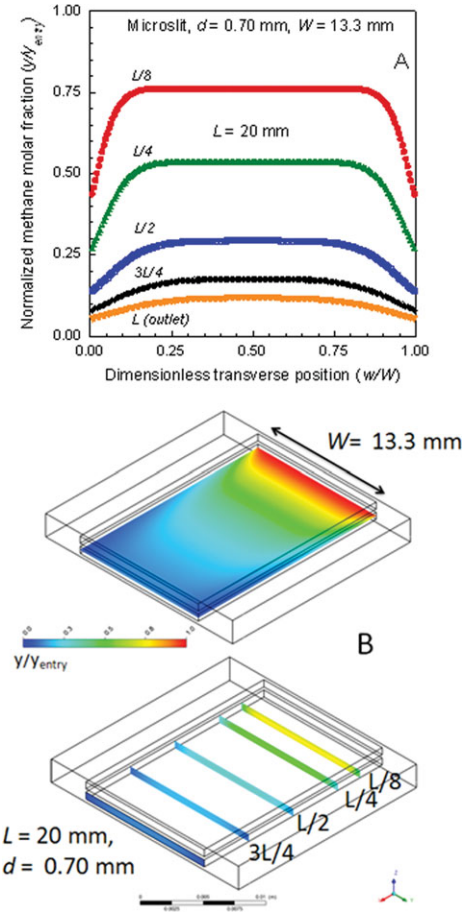

Figure 12. Normalized methane molar fraction in the reforming duct of the microslit with *d* = 0.70 mm at GHSV of 21,048 h^{-1} (WHSV = 2708 h^{-1}) and the indicated positions along the microslit length: profiles along the dimensionless transverse position (A) and colored contours (B).

[Color figure can be viewed in the online issue, which is available at wileyonlinelibrary.com.]

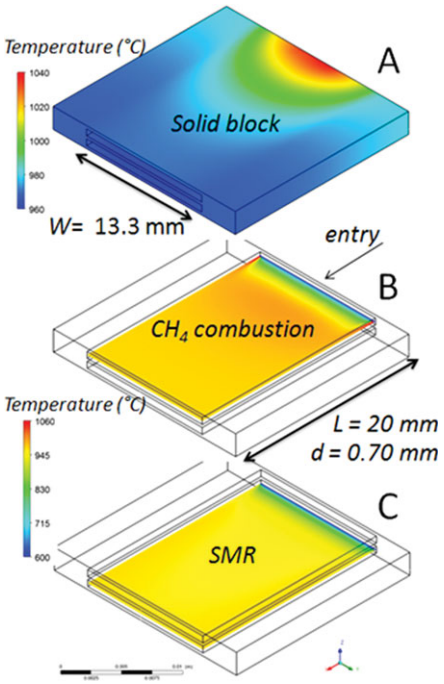

Figure 13. Temperature in the solid block (A) and in a central plane in the methane combustion (B) and SMR (C) ducts of microslits with d = 0.70 mm (SMR GHSV = 21,048 h^{-1}, WHSV = 2708 h^{-1}).

[Color figure can be viewed in the online issue, which is available at wileyonlinelibrary.com.]

where τ is the mean fluid residence time and d_h is the hydraulic diameter. *Bo* numbers have been calculated at the mean SMR temperature of 900°C for the channels with characteristic dimension of 0.70 and 2.80 mm under unfavorable conditions, that is, high GHSV (low τ). It should be noted that for square channels d_h coincides with d. *Bo* number for d = 0.70 mm and GHSV = 40,000 h^{-1} is 10,650 and for d = 2.80 mm and GHSV = 10,000 h^{-1} is 2660. These values are much higher than 100 and therefore, axial dispersion effects are not important.[9] Reynolds numbers (*Re*) for these cases were 24 and 17 so the flow regime was clearly laminar. Nevertheless, as illustrated in Figure 11B for the channel with d = 2.80 mm at Re = 17, a relatively long entrance zone can be observed that is close to half the length of the channel. A similar length of the entrance zone was found for the channel with d = 0.70 mm.

Influence of transport limitations. Microslits

The normalized methane molar fraction along the dimensionless transverse position in a central plane of the microslit with characteristic dimension of 0.70 mm at GHSV = 21,048 h^{-1} is shown in Figure 12A. These results are depicted as colored contours in Figure 12B. The profiles are given at the following positions along the microslit length (L = 20 mm): $L/8$, $L/4$, $L/2$, $3{\cdot}L/4$, and L. Comparing Figures 7A and 12A, it is clear that more intense transverse concentration profiles are established in the microslit than in the microchannel, which can explain the better performance exhibited by the microchannel for a given characteristic dimension. This is due to the fact that in the square microchannel both the width and the height are in the submillimeter scale, whereas in the microslit the width (13.30 mm) is more than one order of magnitude higher than the height (0.70 mm) resulting in more marked transverse transport limitations. The temperatures in the steel block and a central plane of the methane combustion and SMR microslits are shown in the form of colored contours in Figures 13A–C, respectively. The maximum difference of temperature within the block is about 80°C. As concerns the fluidic regions, the methane combustion reaction experiences a temperature peak of about 1060°C, whereas the outlet temperature is around 967°C. In the case of the SMR reaction (Figure 13C), there are very smooth transverse temperature profiles and the reaction takes place almost isothermally at about 959°C along the main part of the slit length.

Finally, the microslit with the biggest characteristic dimension (d = 2.80 mm) at GHSV of 6249 h^{-1} is considered. The evolution of the normalized methane molar fraction for the SMR reaction along the dimensionless transverse position and height is shown in Figures 14A and B, respectively, and in the form of colored contours in Figure 15. When these results are compared with the ones in Figures 12A and B, it can be seen that the concentration profiles become much more intense and that even along the

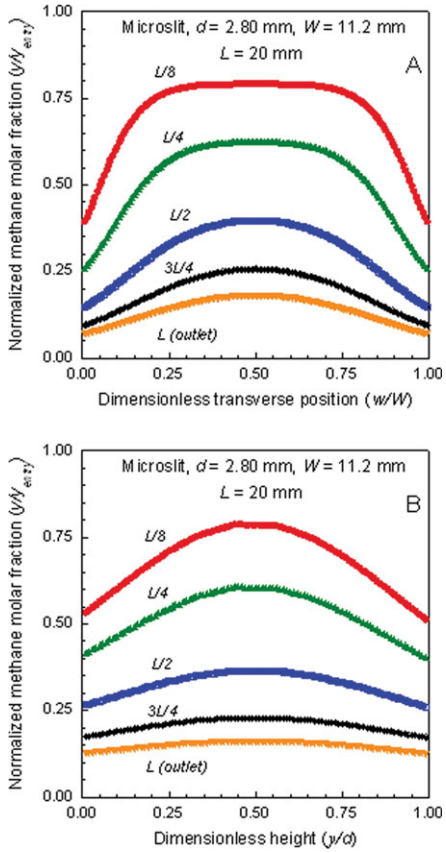

Figure 14. Normalized methane molar fraction in the reforming duct of the microslit with d = 2.80 mm at GHSV of 6249 h^{-1} (WHSV = 2708 h^{-1}) and the indicated positions along the microslit length: profiles along the dimensionless transverse position (A) and dimensionless height (B).

[Color figure can be viewed in the online issue, which is available at wileyonlinelibrary.com.]

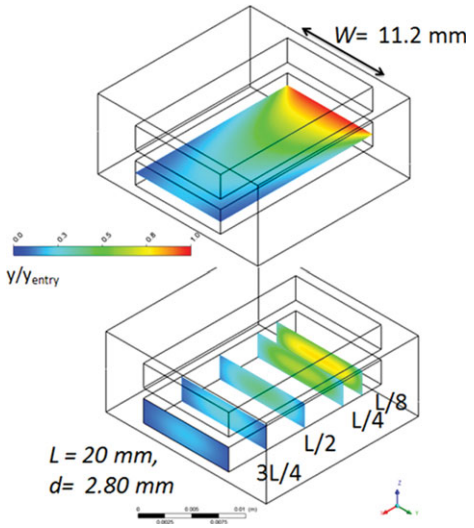

Figure 15. Normalized methane molar fraction in the reforming duct of the microslit with d = 2.80 mm at GHSV of 6249 h^{-1} (WHSV = 2708 h^{-1}) and the indicated positions along the microslit length.

[Color figure can be viewed in the online issue, which is available at wileyonlinelibrary.com.]

characteristic dimension, that is the slit height, significant profiles develop (Figure 14B). As in the case of the microchannels, these mass transport limitations are likely responsible for the remarkable worsening of the microslits performance as the characteristic dimension increases, even within the millimeter scale. Temperature distributions for the biggest microslit are shown in Figures 16A–C. It can be seen that the maximum temperature difference within the solid block, about 20°C, is much lower than for the microslits with d = 0.70 mm. However, the transverse temperature profiles are more marked, when d = 2.80 mm. In the case of the methane combustion reaction, hot points appear close to the walls, whereas the mean combustion outlet temperature is 978°C. Regarding the reforming reaction, transverse temperature profiles appear along the first half length of the microslit. From that point, the reforming reaction progresses almost isothermally at about 955°C.

Mass *Fo* numbers have been also calculated for the microslits according to Eq. 1. Results (not shown) are similar to the ones obtained for the microchannels. For example, *Fo* numbers lower than 1 have been obtained for the largest microslit (d = 2.80 mm) at the space velocities of 6249 and 781 h^{-1}. In the first case, this happens from an axial position of 17.5 mm and in the second one from 19.7 mm. *Bo* numbers have been calculated as well at the mean SMR temperature of 900°C for the slits with characteristic dimension of 0.70 and 2.80 mm according to Eq. 2. The values of the corresponding hydraulic diameters are included in Table 1. *Bo* number for d = 0.70 mm and GHSV = 21,048 h^{-1} is 5607 and for d = 2.80 mm and GHSV = 6249 h^{-1} is 1664. These values are approximately half the values for the microchannels with the same characteristic size but much higher than 100; therefore, axial dispersion effects can be neglected also for the microslits.

In summary, more marked transverse concentration profiles are established in the microslits than in the microchannels. This fact is likely responsible for the worse performance of the microslits. However, the differences between these geometries are small and would not justify discarding the microslits for the SMR reaction, especially, if we consider that they are easier to manufacture. For the systems under consideration, the most influencing feature is the characteristic dimension. As far as it is well below 1 mm, external transport limitations can be neglected but they can become relevant for values of the characteristic dimension not far above that limit. Advanced microchannel architecture and design as the use of engineered and microstructured catalysts (felts, foams, strings, and etc.) can be used to overcome the negative effect of increasing the characteristic dimension of microreactors.[9,13,21,42]

Conclusions

In the field of microreaction technology, it is commonly claimed that the reduction of the characteristic dimension of microreactors enhances the rate of the physical transport processes. As a matter of fact, microreactors are considered ideal tools to investigate the intrinsic chemical kinetics of heterogeneously catalyzed reactions. Although these statements are true, this does not imply that transport limitations can be neglected in a general way.

In this study, CFD simulations have allowed to investigate the effects of the characteristic dimension (d) in the 0.35–2.80 mm range on the performance of catalytic wall microchannels and microslits. It has been found that little differences exist between the performances of these geometries. For both of them, performance improves as d decreases, particularly at high space

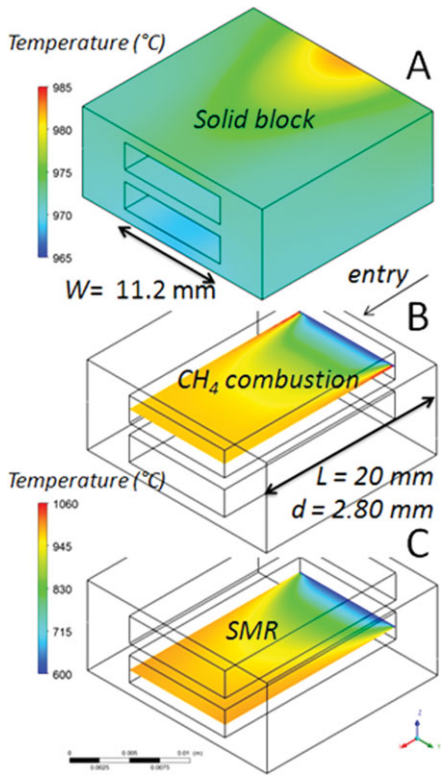

Figure 16. Temperature in the solid block (A) and in a central plane in the methane combustion (B) and SMR (C) ducts of microslits with d = 2.80 mm (SMR GHSV = 6249 h^{-1}, WHSV = 2708 h^{-1}).

[Color figure can be viewed in the online issue, which is available at wileyonlinelibrary.com.]

velocities. It has been found that for the biggest characteristic dimension considered (2.80 mm) the effect of external transport limitations can negatively affect the microreactor performance. In the case of the microslits, marked transverse concentration profiles develop, especially near the microreactor entry. Transport phenomena limitations can be an issue for the steam methane reforming even when using microreactors due to the fast chemical kinetics at the high temperatures at which this reaction is performed.

Acknowledgments

Financial support by the Spanish Ministry of Science and Innovation (ENE2009-14522-C04 grant) is gratefully acknowledged. I. Uriz gratefully acknowledges the fellowships granted by the Innovation Department of the Navarre Government and the Spanish Ministry of Science and Innovation (program FPI, BES-2010-030021).

Notation

Bo = Bodenstein number
c_p = specific heat at constant pressure
d = characteristic dimension
d_h = hydraulic diameter
D = molecular diffusion coefficient
Fo = mass Fourier number
h = specific static enthalpy
L = microreactor length
M = average molecular weight
N_c = number of components
N_r = number of reactions
p = pressure
P_i = partial pressure
R_j = rate of reaction j
R = universal gas constant
Re = Reynolds number
S = source term in conservation equation
T = temperature
$\boldsymbol{u}$ = velocity vector
u_x = axial gas velocity
w = transverse coordinate
W = fluidic region width
x = axial coordinate
y = molar fraction or vertical coordinate
Y = mass fraction

Greek letters

α = aspect ratio
δ = identity matrix
λ = thermal conductivity
μ = dynamic viscosity
υ = stoichiometric coefficient
ρ = density
τ = mean residence time or shear stress

Superscripts and subscripts

E = energy
i = component index
j = reaction index

Literature Cited

1. Song C. *Introduction to hydrogen and syngas production and purification technologies*. In: Liu K, Song C, Subramani V, editors. *Hydrogen and Syngas Production and Purification Technologies*. Hoboken, NJ: AIChE—Wiley, 2010:1–13.
2. Subramani V, Sharma P, Zhang L, Liu K. *Catalytic steam reforming technology for the production of hydrogen and syngas*. In: Liu K, Song C, Subramani V, editors. *Hydrogen and Syngas Production and Purification Technologies*. Hoboken, NJ: AIChE—Wiley, 2010:14–126.
3. Rostrup-Nielsen T. Hydrogen production advances & challenges. *Prepr. Pap.-Am. Chem. Soc., Div. Fuel Chem.* 2006;51:452–454.
4. Bhat SA, Sadhukhan J. Process intensification aspects for steam methane reforming: an overview. *AIChE J*. 2009;55:408–422.
5. Rostrup-Nielsen T. Manufacture of hydrogen. *Catal. Today* 2005; 106:293–296.
6. Panagiotopoulou P, Kondarides DI, Verykios XE. Chemical reaction engineering and catalysis issues in distributed power generation systems. *Ind. Eng. Chem. Res.* 2011;50:523–530.
7. Holladay JD, Wang Y, Jones E. Review of developments in portable hydrogen production using microreactor technology. *Chem. Rev.* 2004;104:4767–4790.
8. Kolb G, Hessel V. Micro-structured reactors for gas phase reactions. *Chem. Eng. J*. 2004;98:1–38.
9. Renken A, Kiwi-Minsker L. Microstructured catalytic reactors. *Adv. Catal*. 2010;53:47–122.
10. Vlachos DG, Caratzoulas S. The roles of catalysis and chemical engineering in overcoming the energy and environment crisis. *Chem. Eng. Sci*. 2010;65:18–29.
11. Mazanec T, Tonkovich AL, Perry S, Fitzgerald S, Arora, R, Rogers A, Yuschak, T. Intensified steam methane reforming in microchannel reactors. *Prepr. Pap.-Am. Chem. Soc., Div. Fuel Chem.* 2006;51:496–500.
12. Mettler MS, Stefanidis GD, Vlachos DG. Scale-out of microreactor stacks for portable and distributed processing: coupling of exothermic and endothermic processes for syngas production. *Ind. Eng. Chem. Res.* 2010;49:10942–10955.
13. Lerou JJ, Tonkovich AL, Silva L, Perry S, McDaniel J. Microchannel reactor architecture enables greener processes. *Chem. Eng. Sci.* 2010;65:380–385.
14. Tonkovich AY, Perry S, Wang Y, Qiu D, LaPlante T, Rogers WA. Microchannel process technology for compact methane steam reforming. *Chem. Eng. Sci*. 2004;59:4819–4824.
15. Tonkovich ALY, Yang B, Perry ST, Fitzgerald SP, Wang Y. From seconds to milliseconds to microseconds through tailored microchannel reactor design of a steam methane reformer. *Catal. Today* 2007; 120:21–29.
16. Seris ELC, Abramowitz G, Johnston AM, Haynes BS. Scaleable, microstructured plant for steam reforming of methane. *Chem. Eng. J*. 2008;135S:S9–S16.
17. Stefanidis GD, Vlachos DG. Millisecond methane steam reforming via process and catalyst intensification. *Chem. Eng. Technol*. 2008; 31:1201–1209.
18. Stefanidis GD, Vlachos DG. High vs. low temperature reforming for hydrogen production via microtechnology. *Chem. Eng. Sci*. 2009;64: 4856–4865.
19. Stefanidis GD, Vlachos DG. Intensification of steam reforming of natural gas: choosing combustible fuel and reforming catalyst. *Chem. Eng. Sci*. 2010;65:398–404.
20. Ryi SK, Park JS, Choi SH, Cho SH, Kim SH. Novel micro fuel processor for PEMFCs with heat generation by catalytic combustion. *Chem. Eng. J*. 2005;113:47–53.
21. Cao C, Wang Y, Rozmiarek RT. Heterogeneous reactor model for steam reforming of methane in a microchannel reactor with microstructured catalysts. *Catal. Today* 2005;110:92–97.
22. Kolios G, Frauhammer J, Eigenberger G. Efficient reactor concepts for coupling of endothermic and exothermic reactions. *Chem. Eng. Sci*. 2002;57:1505–1510.
23. Zanfir M, Gavriilidis A. Catalytic combustion assisted methane steam reforming in a catalytic plate reactor. *Chem. Eng. Sci*. 2003;58: 3947–3960.
24. Vaccaro S, Malangone L, Ciambelli P. Micro-scale reactor for syngas production. *Ind. Eng. Chem. Res.* 2010;49:10924–10933.
25. Vaccaro S, Malangone L, Ciambelli P. Modelling of a catalytic micro-reactor coupling endothermic methane reforming and combustion. *Int. J. Chem. Reactor Eng*. 2010;8; Article A51.
26. Mettler MS, Stefanidis GD, Vlachos DG. Enhancing stability in parallel plate microreactor stacks for syngas production. *Chem. Eng. Sci*. 2011;66:1051–1059.
27. Arzamendi G, Diéguez PM, Montes M, Odriozola JA, Falabella Sousa-Aguiar E, Gandía LM. Methane steam reforming in a microchannel reactor for GTL intensification: a computational fluid dynamics simulation study. *Chem. Eng. J*. 2009;154:168–173.
28. Arzamendi G, Diéguez PM, Montes M, Centeno MA, Odriozola JA, Gandía LM. Integration of methanol steam reforming and combustion in a microchannel reactor for H_2 production: a CFD simulation study. *Catal. Today* 2009;143:25–31.
29. Uriz I, Arzamendi G, López E, Llorca J, Gandía LM. Computational fluid dynamics simulation of ethanol steam reforming in catalytic wall microchannels. *Chem. Eng. J*. 2011;167:603–609.
30. Arzamendi G, Diéguez PM, Montes M, Odriozola JA, Falabella Sousa-Aguiar E, Gandía LM. Computational fluid dynamics study of

heat transfer in a microchannel reactor for low-temperature Fischer–Tropsch synthesis. *Chem. Eng. J.* 2010;160:915–922.
31. Arzamendi G, Uriz I, Diéguez PM, Laguna OH, Hernández WY, Álvarez A, Centeno MA, Odriozola JA, Montes M, Gandía LM. Selective CO removal over Au/CeFe and CeCu catalysts in microreactors studied through kinetic analysis and CFD simulations. *Chem. Eng. J.* 2011;167:588–596.
32. Laguna OH, Ngassa EM, Oraá S, Álvarez A, Domínguez MI, Romero-Sarria F, Arzamendi G, Gandía LM, Centeno MA, Odriozola JA. Preferential oxidation of CO (CO-PROX) over CuO_x/CeO_2 coated microchannel reactor. *Catal. Today*, in press; doi:10.1016/j.cattod.2011.03.024.
33. Almeida LC, Echave FJ, Sanz O, Centeno MA, Arzamendi G, Gandía LM, Sousa-Aguiar EF, Odriozola JA, Montes M. Fischer–Tropsch synthesis in microchannels. *Chem. Eng. J.* 2011;167:536–544.
34. Cruz S, Sanz O, Poyato R, Laguna OH, Echave FJ, Almeida LC, Centeno MA, Arzamendi G, Gandía LM, Souza-Aguiar EF, Montes M, Odriozola JA. Design and testing of a microchannel reactor for the PROX reaction. *Chem. Eng. J.* 2011;167:634–642.
35. Paschedag AR. *Computational fluid dynamics.* In *Ullmann's Modeling and Simulation.* Weinheim: Wiley-VCH Verlag GmbH, 2007:354–357.
36. Rostrup-Nielsen JR. *Catalytic steam reforming*. In: Anderson JR, Boudart M, editors. *Catalysis-Science and Technology*. Berlin: Springer-Verlag, 1984; Vol. 5:p. 51.
37. De Groote AM, Froment GF. Reactor modeling and simulations in synthesis gas production. *Rev. Chem. Eng.* 1995;11:145–183.
38. Kolaczkowski ST, Serbetcioglu S. Development of combustion catalysts for monolith reactors: a consideration of transport limitations. *Appl. Catal. A: Gen.* 1996;138:199–214.
39. Ridler D, Twigg MV. *Steam reforming*. In: Twigg MV, editor. *Catalyst Handbook*. London: Manson Publishing, 1996:p. 271.
40. Kölbl A, Pfeifer P, Schubert K, Fichtner M, Liauw MA, Emig G. Examination of external mass transport in a microchannel reactor by pressure variation. *Chem. Eng. Technol.* 2004;27:671–675.
41. Walter St, Malmberg St, Schmidt B, Liauw MA. Mass transfer limitations in microchannel reactors. *Catal. Today* 2005;110:15–25.
42. Kiwi-Minsker L, Renken A. Microstructured reactors for catalytic reactions. *Catal. Today* 2005;110:2–14.

Manuscript received May 22, 2011, and revision received Sept. 23, 2011.